Do Strong Winds Impact Water Mass, Nutrient, and Phytoplankton Distributions in the Ice-Free Canada Basin in the Fall?

Shigeto Nishino[1], Yusuke Kawaguchi[2], Jun Inoue[3], Michiyo Yamamoto-Kawai[4], Michio Aoyama[5,6], Naomi Harada[1,3,7], and Takashi Kikuchi[1]

[1]Institute of Arctic Climate and Environment Research (IACE), Research Institute for Global Change (RIGC), Japan Agency for Marine-Earth Science and Technology (JAMSTEC), Yokosuka, Japan, [2]Atmosphere and Ocean Research Institute, The University of Tokyo, Kashiwa, Japan, [3]National Institute of Polar Research, Tachikawa, Japan, [4]Tokyo University of Marine Science and Technology, Tokyo, Japan, [5]Global Ocean Observation Research Center (GOORC), Research Institute for Global Change (RIGC), Japan Agency for Marine-Earth Science and Technology (JAMSTEC), Yokosuka, Japan, [6]Center for Research in Isotopes and Environmental Dynamics, University of Tsukuba, Tsukuba, Japan, [7]Earth Surface System Research Center (ESS), Research Institute for Global Change (RIGC), Japan Agency for Marine-Earth Science and Technology (JAMSTEC), Yokosuka, Japan

Abstract In general, strong wind events can enhance ocean turbulent mixing, followed by episodic nutrient supply to the euphotic zone and phytoplankton blooms. However, it is unclear whether such responses to strong winds occur in the ice-free Canada Basin, where the seasonal pycnocline is strong and the nutricline is deep. In the present study, we monitored a fixed-point observation (FPO) station in the Canada Basin for about 3 weeks in the fall of 2014 to examine the oceanic and biological responses to strong winds. At the FPO site, oceanic microstructure measurements, hydrographic surveys, and water sampling were performed with high temporal resolution, recording internal wave propagation, eddy passage, and water mass changes. Strong winds and internal wave propagation significantly enhanced the mixing above and at the seasonal pycnocline, but their effects were diminished at the nutricline, which was much deeper than the seasonal pycnocline. Therefore, wind-induced mixing did not increase the upward nutrient supply from the nutricline and did not impact phytoplankton (chlorophyll *a*) distribution in the surface layer of the FPO site. The temporal evolution of the chlorophyll *a* concentration was most closely related to water mass changes. We also observed prominent subsurface chlorophyll *a* maxima with abundant large-sized phytoplankton that were likely carried by warm-core eddies to the FPO site. Phytoplankton biomass may have been sustained by the high concentration of ammonium within the eddy and ammonium regeneration at the seasonal pycnocline, where particulate organic matter likely accumulated.

Plain Language Summary The Arctic basins, once covered with multiyear ice, are gaining ice-free areas in summer and fall as an effect of global warming. An ice-free upper ocean is more susceptible to wind forcing than ice-covered waters. Here, we studied the oceanic and biological responses to strong winds in the ice-free Canada Basin, where a density gap (pycnocline) was seasonally formed at a depth of about 20 m between the sea surface layer containing sea ice meltwater and the layer below. Although significant wind-induced mixing was observed above and at this seasonal pycnocline, mixing was attenuated at nutricline depths (~60 m), where nutrient concentrations increased strongly with depth. Thus, nutrients were not supplied from the nutricline to the sea surface layer through wind-induced mixing, and phytoplankton biomass did not increase in response to strong winds. However, phytoplankton biomass sometimes increased around the seasonal pycnocline, where ammonium was available for use in photosynthesis. This ammonium was likely supplied by warm-core eddies transporting shelf water into the Canada Basin. Another conceivable source of ammonium was particulate organic matter suspended at the seasonal pycnocline that decomposed, producing ammonium.

1. Introduction

Arctic sea ice extent has rapidly decreased in recent decades, which is a defining feature of Arctic climate change (e.g., Comiso et al., 2017; Serreze et al., 2007; Stroeve et al., 2012). The decrease in sea ice contributes strongly to the freshening of the Arctic Ocean, especially in the Beaufort Gyre of the Canada Basin, as a

result of freshwater accumulation (Proshutinsky et al., 2009; Wang et al., 2018). Freshwater accumulation in the Canada Basin causes deepening of the nutricline (McLaughlin & Carmack, 2010) and can change phytoplankton community structure (Li et al., 2009), decrease phytoplankton production (Coupel et al., 2015), and weaken the biological pump (Nishino, Kikuchi, et al., 2011; Zhuang et al., 2018). However, the activity of oceanic eddies (number, volume, and lifespan) in this region is expected to increase with sea ice loss (Kawaguchi et al., 2012; Watanabe et al., 2012, 2014), and the role of eddies in supplying nutrients laterally and maintaining phytoplankton production appears to be more important than previously thought (Aguilar-Islas et al., 2013; Nishino, Itoh, et al., 2011; Nishino et al., 2018; Yun et al., 2015). On the other hand, the delay in fall freezing of the eastern part of the East Siberian Sea during the late 2000s compared with the early 2000s might have resulted in the formation of a large water mass through cooling and convection, and the spread of this water into the southern Makarov Basin may have caused shoaling of the nutricline (Nishino et al., 2013). Shelf water in the western part of the East Siberian Sea, containing high nutrient concentrations, also spreads into the central Arctic Ocean, forming a shallower nutricline than that in the Canada Basin (Alkire et al., 2019). These shallow nutriclines could convey an advantage for phytoplankton production under decreasing sea ice conditions.

The recent decrease in Arctic sea ice may also significantly amplify upper ocean responses to atmospheric forcing, such as wind-induced ocean mixing (e.g., Kawaguchi et al., 2015; Rainville et al., 2011; Rainville & Woodgate, 2009). In addition, because a later freeze-up is expected, the sea surface would be exposed to fall storms for a longer period of time (e.g., Figure 9.13 in Loeng et al., 2005). The frequency and intensity of cyclones in the Arctic are generally increasing, and storm tracks may shift northward (e.g., McCabe et al., 2001; Orlanski, 1998; Sepp & Jaagus, 2011; Serreze et al., 2000; Zhang et al., 2004). These effects could induce a second phytoplankton bloom in the fall (fall bloom), as the delayed freeze-up and increased exposure of the sea surface to fall storms lead to significant wind-induced vertical mixing and upward supply of nutrients, increasing phytoplankton biomass. Ardyna et al. (2014) used satellite data to show that the frequency and area of fall blooms have recently increased throughout the Arctic. Nishino et al. (2015) reported an increase in vertical nutrient fluxes and the accompanying fall bloom during strong wind events in the Chukchi Sea based on observational evidence. Such an increase in biomass during the fall bloom could be associated with changes in phytoplankton and zooplankton communities, with impacts on higher trophic levels in the ecosystem (Fujiwara et al., 2018; Matsuno et al., 2015; Yokoi et al., 2016).

Although strong wind events can impact ocean turbulent mixing and the marine ecosystem in the seasonally ice-free Chukchi Sea as described above, it remains unclear whether similar responses to strong wind events occur in the ice-free Canada Basin. In early to midsummer (from beginning of June to mid-August), sea ice meltwater is injected into the surface layer of the Canada Basin, resulting in the formation of a seasonal halocline (pycnocline) with the strongest stratification in the water column (Jackson et al., 2010; McPhee et al., 1998). In general, turbulent mixing is rapidly attenuated under such a strong stratification (e.g., Randelhoff et al., 2014, 2017). Lincoln et al. (2016) observed that turbulence was not energetic below the stratified upper layer despite the unusually ice-free and stormy summer of 2012 in the Canada Basin.

The nutricline in the Canada Basin is formed by lateral advection of nutrient-rich Pacific-origin water under a layer in which nutrients are decreased (nitrate is depleted) by phytoplankton production (Carmack et al., 2004; Codispoti et al., 2005; McLaughlin & Carmack, 2010). The lateral advection of Pacific-origin water also maintains the upper part of permanent halocline structures (Aagaard et al., 1981; Killworth & Smith, 1984). The depth of the nutricline (upper permanent halocline) is deeper than that of the seasonal halocline, and thus, the nutricline may not be influenced by the wind-induced mixing that is largely weakened in the seasonal halocline (Lincoln et al., 2016; Randelhoff et al., 2014, 2017). A field study conducted in the southeast Beaufort Sea suggested that wind-induced mixing did not increase nutrient concentrations in the surface layer in the fall due to the presence of a strong stratification, despite the episodic passage of storms over the study area (Tremblay et al., 2008). On the other hand, Randelhoff et al. (2016) showed that nitrate fluxes across the nutricline increased when the ocean (around the Svalbard shelf slope) changed from ice-covered to ice-free conditions. The main cause of this increase in the nitrate fluxes was not an enhancement of wind-induced mixing but rather a weak stratification at the nutricline during the ice-free condition. In the Canada Basin, a year-round mooring indicated that the kinetic energy of internal waves increased in summer and fall, particularly during months in which ice diminished or was formed, compared with wave energy
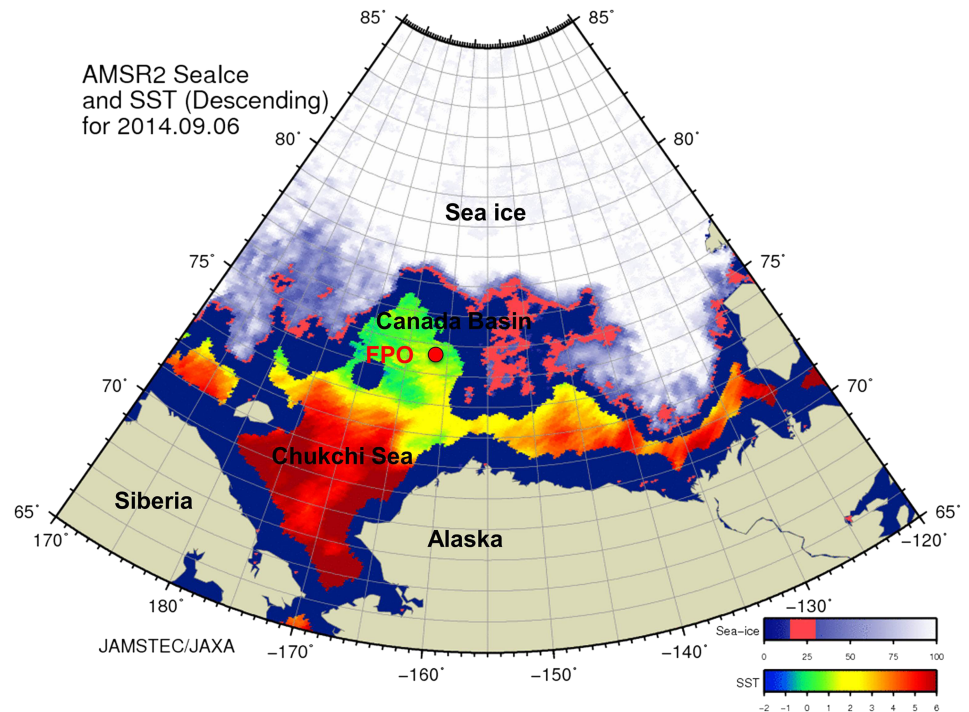
Figure 1. Map of the fixed-point observation (FPO) station with sea ice concentration and sea surface temperature (SST) on 6 September 2014, the first day of observation. The FPO site was located at 74.75°N, 162°W in the Canada Basin. Sea ice and SST data were derived from the Advanced Microwave Scanning Radiometer 2 (AMSR2) and provided by the Japan Aerospace Exploration Agency (JAXA).

during the ice-covered winter season (Kawaguchi et al., 2019), but did not provide data showing a relationship between this wave energy and nutrient fluxes. Some model results suggest that continued thinning of the ice cover in the Canada Basin might leave the ice too thin and fragile to provide a barrier to momentum flux (Steiner et al., 2016). In that case, mixing may break up the strong stratification in the Canada Basin, causing near-surface waters to become saltier and potentially enhancing the nutrient supply. Kawaguchi et al. (2016) found that notable turbulent mixing occurred in the lower halocline layer during the transit of an anticyclonic cold-core eddy across a fixed-point observation (FPO) site in the seasonally ice-free Northwind Abyssal Plain (NAP) of the Canada Basin. Such subsurface turbulent mixing below the upper permanent halocline might influence nutrient fluxes and phytoplankton distribution.

The present study demonstrates the responses of nutrient and phytoplankton distributions in the Canada Basin to wind forcing and physical oceanographic processes such as turbulent mixing, eddies, and currents. Using an Eulerian approach, we established an FPO station for approximately 3 weeks during fall 2014 in the seasonally ice-free NAP of the Canada Basin (74.75°N, 162°W; see Figure 1), where atmospheric and physical oceanographic conditions were previously studied by Inoue et al. (2018) and Kawaguchi et al. (2016), respectively. At the FPO station, high temporal resolution surveys were performed using an ocean microstructure profiler, conductivity-temperature-depth (CTD) sensors, and Niskin bottles (see section 2) to detect internal wave propagation, eddy passage, and water mass changes that may influence the ecosystem of the Canada Basin. As the basis of ecosystem assessment, we focused mainly on water mass and nutrient and phytoplankton distributions and their temporal changes at the FPO station (see section 3). Based on analysis of data from the FPO, we discuss the present state and future scenarios of ecological responses to sea ice reduction in the Canada Basin (section 4) and then summarize the present study (section 5).

2. Data and Methods

2.1. R/V *Mirai* Arctic Cruise 2014

We conducted meteorological and hydrographic surveys from late summer through fall 2014 (31 August to 10 October) over the Chukchi Sea and the Canada Basin (Figure 2), onboard the R/V *Mirai* of the Japan
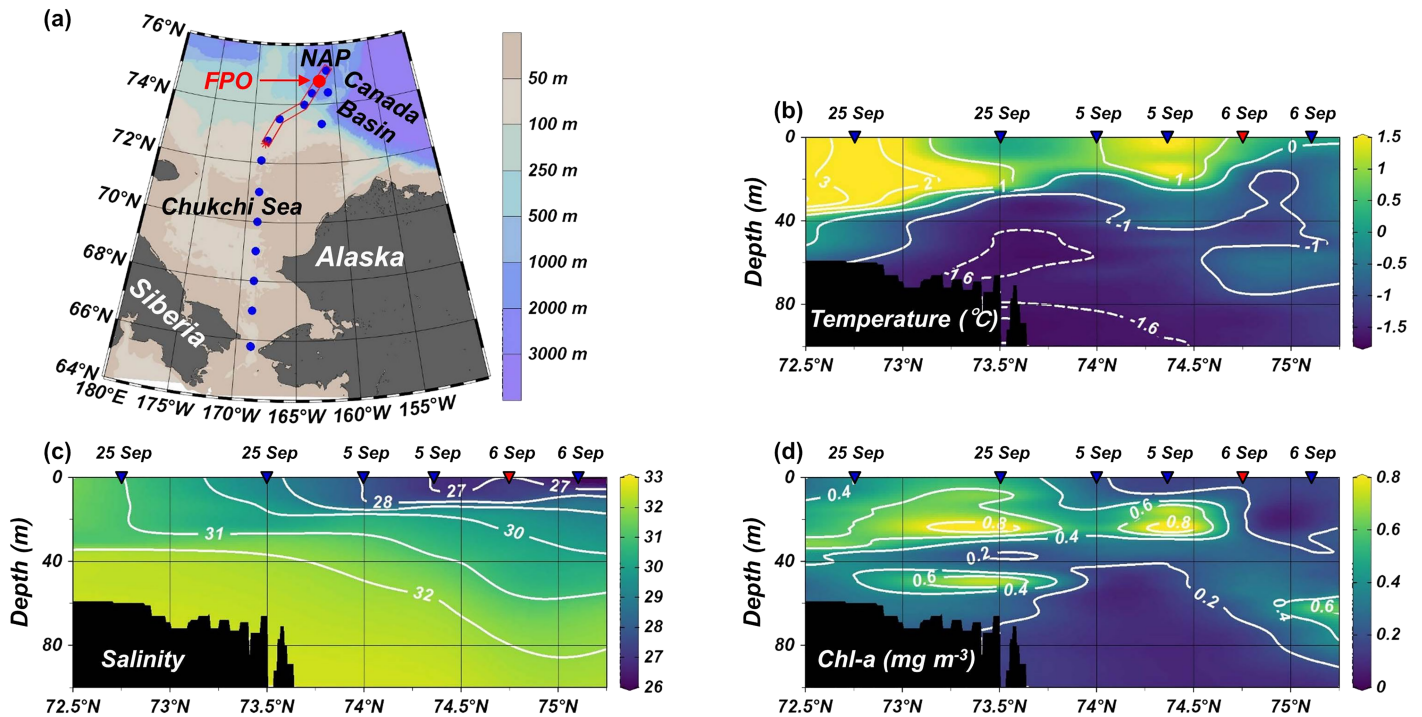
Figure 2. (a) Hydrographic stations and the FPO site; vertical sections of (b) temperature (°C), (c) salinity, and (d) chlorophyll *a* (fluorescence) (mg/m³) at hydrographic stations between 72.5°N and 75.5°N. In (a), conductivity-temperature-depth (CTD) measurements were conducted at stations indicated with blue dots, whereas the FPO site is shown with a red dot. The Northwind Abyssal Plain is abbreviated to NAP. The data obtained from hydrographic stations within the red rectangle were used to construct the vertical sections shown in (b)–(d). In (b)–(d), all data were obtained from sensors attached to the CTD equipment. Blue inverted triangles at the top of each panel indicate the hydrographic stations, and the red inverted triangle represents the FPO site. The observation dates for each station are shown above the inverted triangles. The data at the FPO site are those from 6 September, which was the first day of the FPO, for the drawings of the vertical sections. Note that the data from the Chukchi Sea (two stations on the shallower side) were obtained after completion of the FPO and thus have a time lag compared with the basin-side data.

Agency for Marine-Earth Science and Technology (JAMSTEC). During the surveys, we established an FPO station in the seasonally ice-free NAP of the Canada Basin (74.75°N, 162°W; Figures 1 and 2a), which was sampled for about 3 weeks (6–24 September). At the FPO station, continuous surface meteorological observations, ocean microstructure measurements (every 6 hr), CTD (every 6 hr), and water sampling (every 12 hr) were undertaken (some casts were canceled due to rough weather). Expendable CTD (XCTD) surveys were also conducted to monitor the water mass distribution at 1.5- to 18-km intervals between 74°N and 75°N around 162°W, including at the FPO station. Ocean currents were continuously monitored using a shipboard acoustic Doppler current profiler (ADCP). Detailed descriptions of data acquisition during the cruise are presented in the cruise report (Inoue, 2014), and the data were released via the Data and Sample Research System for Whole Cruise Information (DARWIN) of JAMSTEC (http://www.godac.jamstec.go.jp/darwin/cruise/mirai/mr14-05/e). The following section outlines how each observation was collected.

2.2. Surface Wind Observations

Surface meteorological parameters were observed throughout the cruise. In this study, we used wind speed and direction data at the FPO station. These data were obtained with an anemometer (KE-500, Koshin Denki Kogyo Co., Ltd., Tokyo, Japan) installed on the foremast of the ship at a height of 24 m above the sea surface. The data were averaged over 3-hr periods.

2.3. Ocean Microstructure Measurements

To measure ocean turbulent mixing, microscale (0.001–1 m) vertical shear data were collected using a Turbulent Ocean Microstructure Acquisition profiler (TurboMAP, JFE Advantech Co., Ltd., Nishinomiya, Japan; Wolk et al., 2002), which was lowered from the ship (R/V *Mirai*) to a depth of approximately

400 m. Within the top 7 m, microscale data were not used for analysis, as they may have been affected by the initial adjustment to a free-falling state. The dissipation rate of turbulent kinetic energy, ε, was calculated from small-scale current shear by integrating the energy spectrum into the wavenumber field. The details of this calculation were described by Kawaguchi et al. (2016).

2.4. CTD and Water Sampling

A CTD system (SBE9plus, Sea-Bird Electronics, Inc., now Sea-Bird Scientific, Bellevue, WA, USA) equipped with 36 Niskin bottles (12 L) was used to collect samples and make observations. Sensors including a fluorometer (Seapoint Chlorophyll Fluorometer, Seapoint Sensors, Inc., Exeter, NH, USA) and a transmissometer (C-Star, WET Labs, Inc., now Sea-Bird Scientific, Philomath, OR, USA) were attached to the CTD system. Seawater samples were collected for measurement of salinity, dissolved oxygen, total alkalinity, nutrients (nitrate, nitrite, phosphate, silicate, and ammonium), total and size-fractionated chlorophyll a, and other chemical and biological parameters.

Bottle salinity samples were analyzed following the Global Ocean Ship-based Hydrographic Investigations Program (GO-SHIP) Repeat Hydrography Manual using a salinometer (Guildline AUTOSAL 8400B, OSIL, Havant, UK) and International Association for the Physical Sciences of the Oceans standard seawater as a reference material (Kawano, 2010). The precision of salinity measurements was 0.0131 for shallow-water samples ($\leq$200 m) and 0.0007 for deep water samples ($>$200 m). Bottle salinity data were used to calibrate the CTD conductivity sensor.

Dissolved oxygen in the samples was measured through Winkler titration following the World Ocean Circulation Experiment Hydrographic Program method (Dickson, 1996). The precision of dissolved oxygen measurement was 0.23 μmol/kg.

Total alkalinity in the samples was measured with a spectrophotometric system using the protocol reported by Yao and Byrne (1998). Total alkalinity values were calibrated against a certified reference material provided by Dr. Dickson of the Scripps Institute of Oceanography. The precision of total alkalinity measurement was 2.37 μmol/kg.

Nutrient samples were analyzed according to the GO-SHIP Repeat Hydrography Manual (Hydes et al., 2010) using reference materials for nutrients in seawater (Aoyama & Hydes, 2010; Sato et al., 2010). The precision was expressed as the coefficient of variation, which was 0.08% for nitrate, 0.14% for nitrite, 0.14% for phosphate, 0.11% for silicate, and 0.19% for ammonium.

Chlorophyll a in seawater samples was measured with a fluorometric nonacidification method (Welschmeyer, 1994) using a fluorometer (10-AU-005, Turner Designs, San Jose, CA, USA). For size-fractionated chlorophyll a measurements, phytoplankton cells in water samples were fractionated using three types of 47-mm-diameter filters (pore sizes: 20, 10, and 2 μm) and a 25-mm-diameter Whatman GF/F filter (pore size: ~0.7 μm). Although the frequency of observations of total chlorophyll a at the FPO station was every 12 hr (the same as other bottle samples described above), size-fractionated chlorophyll a was measured only once a day. The sampled chlorophyll a data were used to calibrate the fluorometer attached to the CTD system.

For water mass analysis, we used the fraction of sea ice meltwater (f_{SIM}) and other freshwater (f_{OF}) calculated from the relationship between total alkalinity and salinity, as reported by Yamamoto-Kawai et al. (2005). They assumed that other freshwater included river runoff, precipitation, and freshwater carried in Pacific-origin water. The f_{SIM} increases when seawater is influenced by sea ice melt in summer and decreases when seawater is influenced by sea ice formation in winter. A negative f_{SIM} indicates that sea ice formation, which removes freshwater and ejects brine into seawater, is dominant over sea ice melting.

2.5. XCTD

XCTD probes (XCTD-1, Tsurumi-Seiki Co., Ltd., Yokohama, Japan) were launched from the stern of the ship into the sea to obtain vertical profiles of temperature and salinity to a depth of 1,000 m or to the sea bottom in areas where the bottom depth was less than 1,000 m. The data were communicated to a digital data converter and a computer onboard the ship through a fine wire, which is designed to break when the probe reaches its maximum depth. The precision of temperature and salinity measurements was 0.02 and 0.04 °C, respectively.

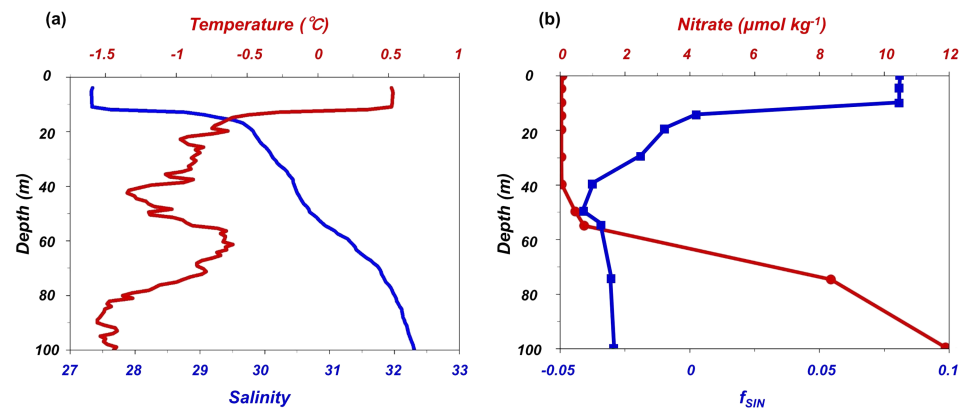**Figure 3.** Vertical profiles of (a) temperature (°C), salinity, (b) nitrate (μmol/kg), and the fraction of sea ice meltwater (f_{SIM}) on 6 September at the FPO site. In (a), the data were obtained from sensors attached to the CTD equipment. In (b), the data were obtained via water sampling and plotted at the levels indicated by the dots.

2.6. ADCP

Throughout the cruise, horizontal current velocities were measured using a shipboard ADCP (75-kHz Ocean Surveyor, Teledyne RD Instruments, Poway, CA, USA) installed on the bottom of the ship's hull. The current speed and direction were obtained over a depth range of 20–250 m with 8-m vertical binning every 5 min. The measured currents were decomposed into eastward (u) and northward (v) components, from which the ship's velocity was subtracted. According to the manufacturer, the accuracy of horizontal velocity observation was ±0.2 cm/s.

3. Results

3.1. Water Mass Distribution at and Around the FPO Site

The FPO site in the NAP portion of the Canada Basin (74.75°N, 162°W) was located in a region where the surface water was characterized by lower temperature, lower salinity, and lower chlorophyll *a* concentration compared with shelf water south of ~74.5°N (Figure 2). At the FPO site, below the surface water, temperature showed a subsurface minimum and maximum at depths of 40–50 and 60–70 m, respectively (Figures 2b and 3a). The salinity of the surface water was extremely low, and a sharp halocline was found below the surface mixed layer (Figures 2c and 3a). Another halocline appeared below the temperature minimum (Figure 3a). The f_{SIM} in the surface mixed layer was extremely high (Figure 3b), and thus, the sharp halocline below it was likely formed seasonally by the surface cover of sea ice meltwater during the summer to fall. This sharp halocline is generally called a seasonal or summer halocline (Jackson et al., 2010; McPhee et al., 1998). We use the term seasonal halocline and refer to the corresponding pycnocline as a seasonal pycnocline. On the other hand, the temperature minimum (40–50 m) corresponded to the f_{SIM} minimum (<0), suggesting a large influence of brine rejection in winter. Thus, this temperature minimum is likely a remnant of the previous winter's mixed layer. Below the temperature minimum, the temperature maximum (60–70 m) water had salinities of 31–32 (Figures 2c and 3a), and this temperature maximum water was identified as Pacific summer water (Coachman et al., 1975; Coachman & Barnes, 1961; Shimada et al., 2001). Below this water, colder water was present, which was associated with Pacific winter water (Aagaard et al., 1981; Coachman & Barnes, 1961; Shimada et al., 2005). The lowest temperature (< −1.6°C) of Pacific winter water was found near the bottom of the shelf and shelf slope south of ~74.5°N (Figure 2b). The halocline maintained by the advection of these Pacific-origin waters is permanent (below~50 m in Figure 3a) and accompanies a nutricline, as shown in Figure 3b.

Based on the chlorophyll *a* distribution (Figure 2d), the FPO site was in a transition zone from the Chukchi Sea to the Canada Basin. South of the FPO site, shelf water with high chlorophyll *a* concentrations extended from the Chukchi Sea. Meanwhile, north of the FPO site in the Canada Basin, the chlorophyll *a* concentration above ~40 m decreased to <0.2 mg/m^3, but the maximum subsurface chlorophyll *a* was found at a depth of ~60 m.
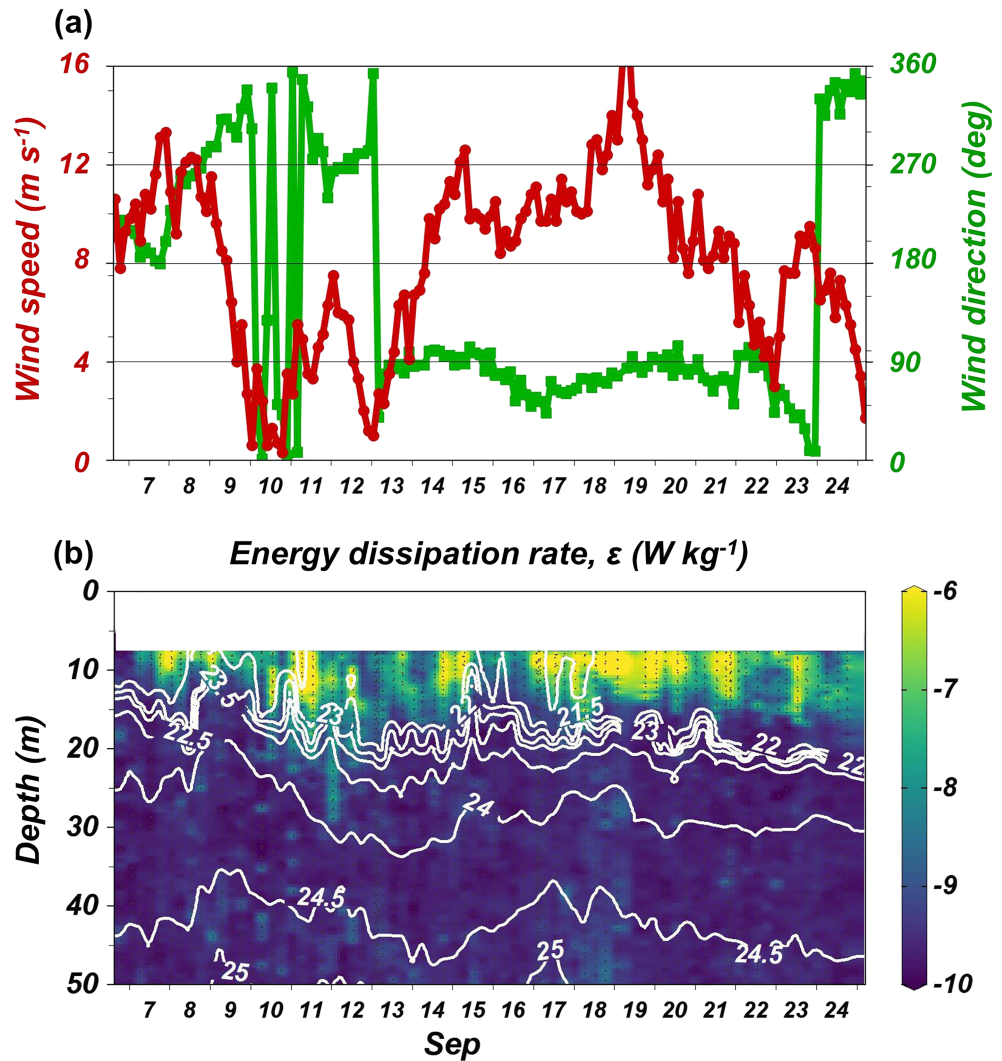
Figure 4. Time series of (a) wind speed (m/s; red) and direction, rotating clockwise from north (degrees; green) and (b) profiles of the kinetic energy dissipation rate, ε (W/kg; color shading), at the FPO station. In (b), ε values are presented on a logarithmic scale, and the color bar on the right indicates the order of magnitude of ε. Contours of potential density, σ_θ (kg/m^3), are superimposed on the temporal evolution of ε.

3.2. FPO: Wind and Ocean Microstructure Measurements

A time series of wind speed and direction during the FPO study is shown in Figure 4a. At the beginning of the FPO (6–9 September), southerly to westerly winds blew strongly at speeds of more than 8 m/s. Subsequently (10–13 September), conditions were calm with almost no wind. Then (14–21 September) we observed easterly winds stronger than 8 m/s. Finally (22–24 September), the wind decreased to less than 8 m/s.

Figure 4b shows a time series of vertical profiles of the turbulent kinetic energy dissipation rate, $\log_{10}$ (ε). The magnitude of ε in the surface layer above the seasonal pycnocline (<~20 m) was large, for example, during the strong easterly wind from 14 to 21 September. Note that high ε values in the surface layer and below the seasonal pycnocline were observed on 11–12 September, despite the calm wind conditions. These high ε values were likely caused by mixing associated with internal waves that accompanied an anticyclonic cold-core eddy on its passage through the FPO site (Kawaguchi et al., 2016).
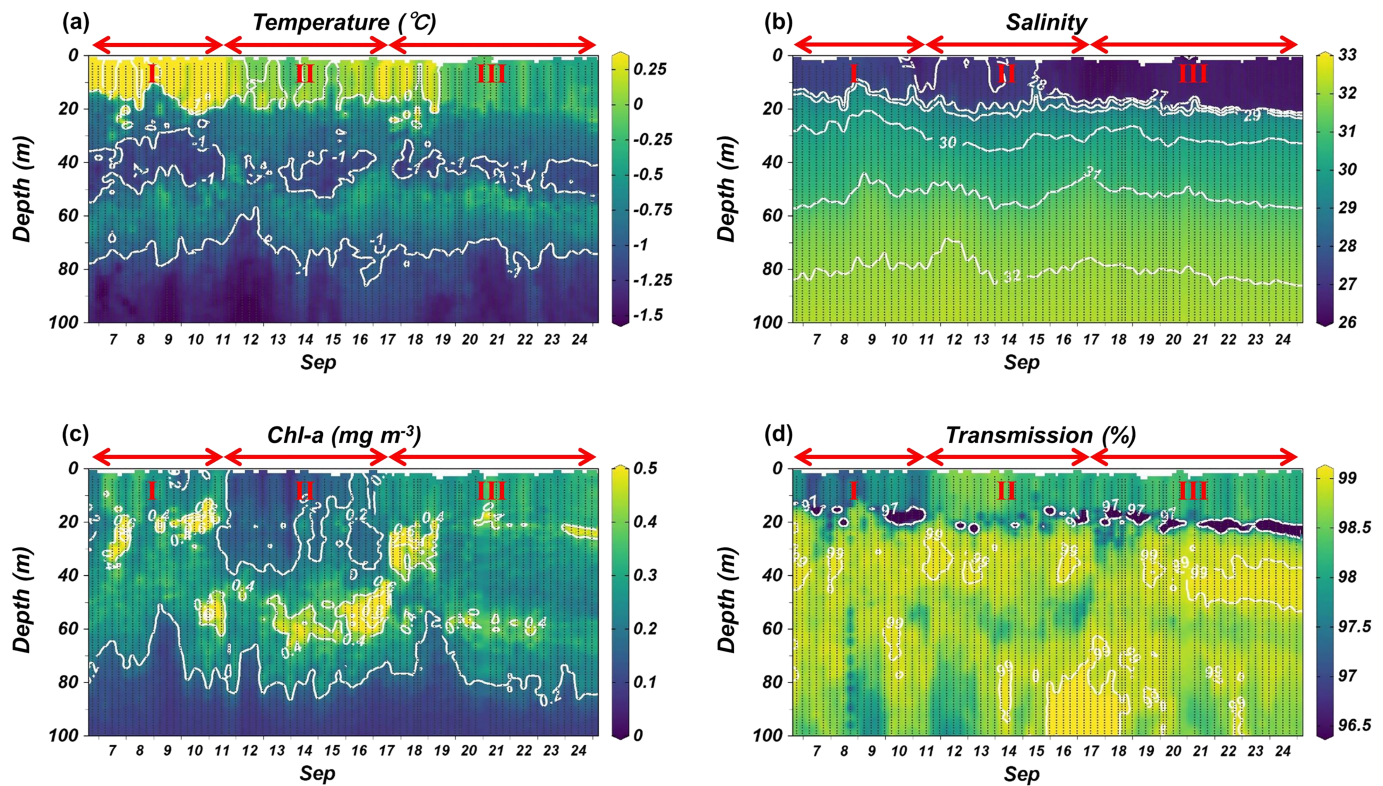
Figure 5. Time series of profiles of (a) temperature (°C), (b) salinity, (c) chlorophyll *a* (fluorescence) (mg/m³), and (d) transmission (%) at the FPO station. All data were obtained using sensors attached to the CTD profiler and were plotted at 1-m intervals, as indicated by the vertical dotted lines in each panel. The labels I, II, and III with arrows at the top of each panel indicate the three terms of the FPO period with differing surface water characteristics.

3.3. FPO: CTD and Water Sampling

A time series of CTD profiles (temperature, salinity, chlorophyll *a*, and transmission) is depicted in Figure 5. Based on CTD observations, the FPO period was divided into three terms. During the first term (Term-I; 6–11 September), the surface water (<~20 m) was warmer, saltier, higher in chlorophyll *a*, and had lower transmission compared to those in the following two terms. The surface water was replaced by water that was colder, fresher, lower in chlorophyll *a*, and had higher transmission during the second term (Term-II; 11–17 September). The surface water of the third term (Term-III; 17–24 September) showed further cooling and freshening, while its chlorophyll *a* concentration increased.

The time series of temperature (Figure 5a) shows a persistent temperature maximum at a depth of ~60 m, where the salinity was 31–32 (Figure 5b), in water classified as Pacific summer water (Coachman et al., 1975; Coachman & Barnes, 1961; Shimada et al., 2001). Below this water lies Pacific winter water (Aagaard et al., 1981; Coachman & Barnes, 1961; Shimada et al., 2005). On 11–13 September, we found extremely low temperatures below a depth of 80 m and salinity of 32 (see Figures 5a and 5b). These samples contained Pacific winter water trapped within an anticyclonic cold-core eddy that was passing through the FPO site (Kawaguchi et al., 2016).

The chlorophyll *a* concentration (Figure 5c) reached its maximum at ~20 m during Term-I, whereas the maximum appeared at ~60 m during Term-II. In Term-III, the chlorophyll *a* concentration showed both shallower and deeper maxima, but their chlorophyll *a* concentrations were relatively low.

In the time series of transmission (Figure 5d), extremely low values appeared at ~20 m during Term-I and Term-III, coinciding with the shallower chlorophyll *a* maximum. The transmission also showed a minimum at ~60 m, where the deeper chlorophyll *a* maximum was found, but this minimum was not as low as that observed at the shallower chlorophyll *a* maximum. In the Pacific winter water layer below ~80 m, transmission tended to be low when the temperature was low, with no signal corresponding to an elevated chlorophyll *a* level. Thus, this low transmission implies that the water there contained fine sediment particles,
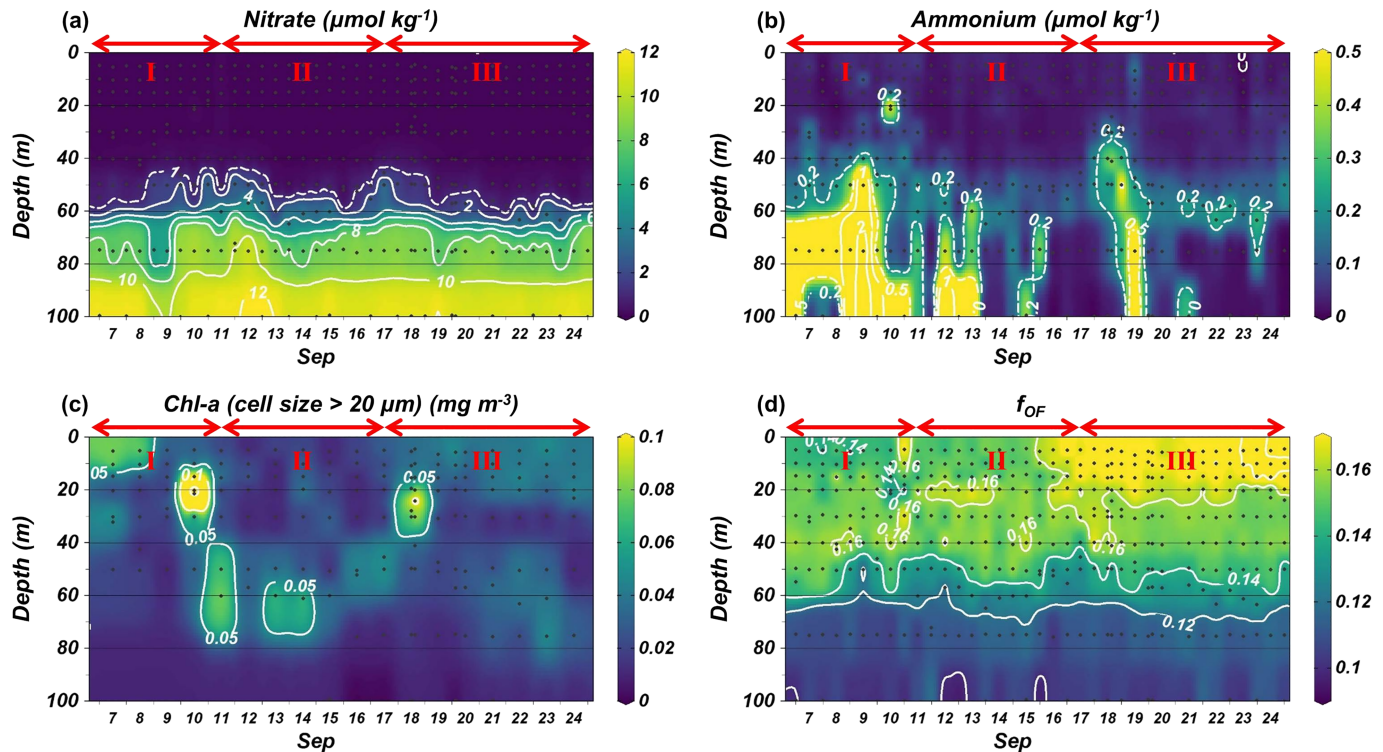
Figure 6. Time series of profiles of (a) nitrate (μmol/kg), (b) ammonium (μmol/kg), (c) large-sized phytoplankton (cell size >20 μm) chlorophyll a (mg/m^3), and (d) fraction of freshwater other than sea ice melt, f_{OF}, at the FPO station. All data were obtained through water sampling, and plotted at the levels indicated by dots in each panel. The labels I, II, and III with arrows at the top of each panel are the same as in Figure 5.

probably derived from the bottom of the Chukchi shelf or the shelf slope, where the Pacific winter water with the lowest temperature was present (Figure 2b).

The time series of sampled water characteristic profiles (nitrate, ammonium, chlorophyll a from large phytoplankton of cell size >20 μm, and the fraction of freshwater other than sea ice melt, f_{OF}) are displayed in Figure 6. Nitrate in the surface water (<~20 m) was depleted throughout the FPO period (Figure 6a). The nitracline appeared at a depth of ~60 m and thus coincided with the temperature maximum of Pacific summer water (Figure 5a), the upper permanent halocline (Figure 5b), the deeper chlorophyll a maximum during Term-II and Term-III (Figure 5c), and the corresponding transmission minimum (Figure 5d). There was no apparent episodic event in the nitrate distribution. On the other hand, we found a sample with a high concentration of ammonium at ~20 m on 10 September (Figure 6b). The ammonium concentration was also elevated in the Pacific winter water layer during the first half of the FPO period, particularly on 9, 12, and 13 September, when the temperature and transmission were both low (see Figures 5a and 5d, respectively). As shown in Figure 2b, we found the lowest-temperature Pacific winter water at the bottom of the shelf and shelf slope south of ~74.5°N. Thus, such water likely obtained ammonium and sediment particles (low transmission) from the bottom and then spread into the Canada Basin (Nishino et al., 2005).

Chlorophyll a of large-sized phytoplankton (cell size >20 μm) was high in the high-ammonium sample collected at ~20 m on 10 September (Figure 6c). Large-sized phytoplankton were also abundant at ~25 m on 18 September, when the ammonium concentration was nearly zero. In both of the samples with abundant large-sized phytoplankton, the temperature and chlorophyll a concentrations were very high (vertical maxima) and transmission was extremely low (vertical minimum).

The time series of f_{OF} profiles (Figure 6d) indicates that the f_{OF} in the surface water (<~20 m) increased as time progressed. On the other hand, the f_{SIM} (not shown) remained nearly unchanged in the surface water during the FPO period. These freshwater behaviors may be related to the temporal change in surface water salinity, which is discussed in section 4.

3.4. XCTD and ADCP Surveys

Just before initiation of the FPO period (on 5–6 September), we conducted XCTD and ADCP surveys between 74°N and 75°N in transit to the FPO station to identify the mesoscale structures of water masses and currents (Figure 7). Vertical sections of temperature and salinity (Figures 7a and 7b) show that the water mass distribution was similar to that at the FPO site, as described above. The salinity contours (isohalines) deepened toward the north, suggesting westward flow in general, except in the surface layer (<~50 m) and around 74.6°N (Figure 7c). Surface water was driven by the southwesterly wind (Figure 4a), and the resultant eastward flow is apparent in the surface layer in Figure 7c. Another area of eastward flow around 74.6°N was associated with an anticyclonic warm-core eddy found between 74.4°N and 74.6°N, as shown in Figure 7a. Within this eddy, a subsurface temperature maximum at ~40 m was prominent, and the Pacific winter water located below the temperature maximum appears to have been strongly modified by the warm water. The 33 and 34 isohalines formed a bowl-shaped structure between 74.4°N and 74.6°N (Figure 7b), which was consistent with the presence of an anticyclonic eddy in this region (Figure 7c).

We also conducted XCTD and ADCP surveys around the FPO site immediately after the appearance of abundant large-sized phytoplankton on 18 September to characterize the oceanic conditions at that time. The observation line was the same as that shown in Figure 7, but the latitudinal range was 74.5°N to 75°N (Figure 8). The vertical section of temperature (Figure 8a) showed subsurface temperature maxima at ~20 and 50 m at 74.7°N near the FPO site, and the Pacific winter water below the temperature maxima was largely modified to be warmer than its surroundings. This temperature distribution indicates the presence of an anticyclonic warm-core eddy at the FPO site. However, the 33 and 34 isohalines deepened toward the north around the FPO site (Figure 8b), where the currents were westward (Figure 8c). Thus, the circulation of the anticyclonic warm-core eddy would have been attenuated and the remnant of the eddy likely drifted with the background westward flow. Note that westward flow at depths shallower than ~50 m was strong, including at the FPO site. These findings are consistent with the strong easterly wind blowing over the FPO site at that time (Figure 4a).

4. Discussion

4.1. Interpretation of Temporal Changes in Surface Water Characteristics

The surface water at the FPO site varied during the study period, as shown in Figure 5. The temperature and salinity of the surface water decreased over time (Figures 5a and 5b). The observed temperature decrease may have been partially caused by ocean heat loss to the atmosphere in the fall cooling season. However, the salinity decrease cannot be explained by fall cooling. If such cooling were accompanied by vertical mixing, the salinity of the surface layer would increase due to mixing with high-salinity water below. Therefore, lateral advection of freshwater is the most plausible scenario driving the decrease in surface water salinity. However, f_{SIM} was nearly constant in the surface water during the FPO period, despite the FPO site being near the ice edge (Figure 1). On the other hand, f_{OF} at the FPO site increased in the surface layer, but was almost unchanged below it, and finally reached a maximum in the surface layer during Term-III (Figure 6d). Therefore, freshwater other than sea ice meltwater was likely supplied laterally to the surface layer, resulting in the decrease in surface water salinity during the FPO period.

Between Term-I and Term-II, significant changes in temperature (Figure 5a), chlorophyll a (Figure 5c), and transmission (Figure 5d) were observed in the surface layer. Water characterized by higher temperature, higher chlorophyll a, and lower transmission occupied the surface layer during Term-I compared to Term-II. As shown in Figure 2, such surface water at the FPO site appears to be influenced by warm shelf water with high chlorophyll a and low transmission (not shown). On the other hand, north of the FPO site, lower temperature (Figure 2b), lower chlorophyll a (Figure 2d), and higher transmission (not shown) were observed in the surface layer. This basin-side water may have been advected to the FPO site, replacing the surface water from Term-I with Term-II water, which was characterized by lower temperature, lower chlorophyll a, and higher transmission. This surface water replacement occurred on 11 September, when weak northerly winds blew over the FPO site (Figure 4a).

Between Term-II and Term-III, surface water salinity decreased (Figure 5b) in response to the increase in f_{OF} (Figure 6d), and chlorophyll a increased in the surface layer, with two peaks occurring at 20–25 and 60 m
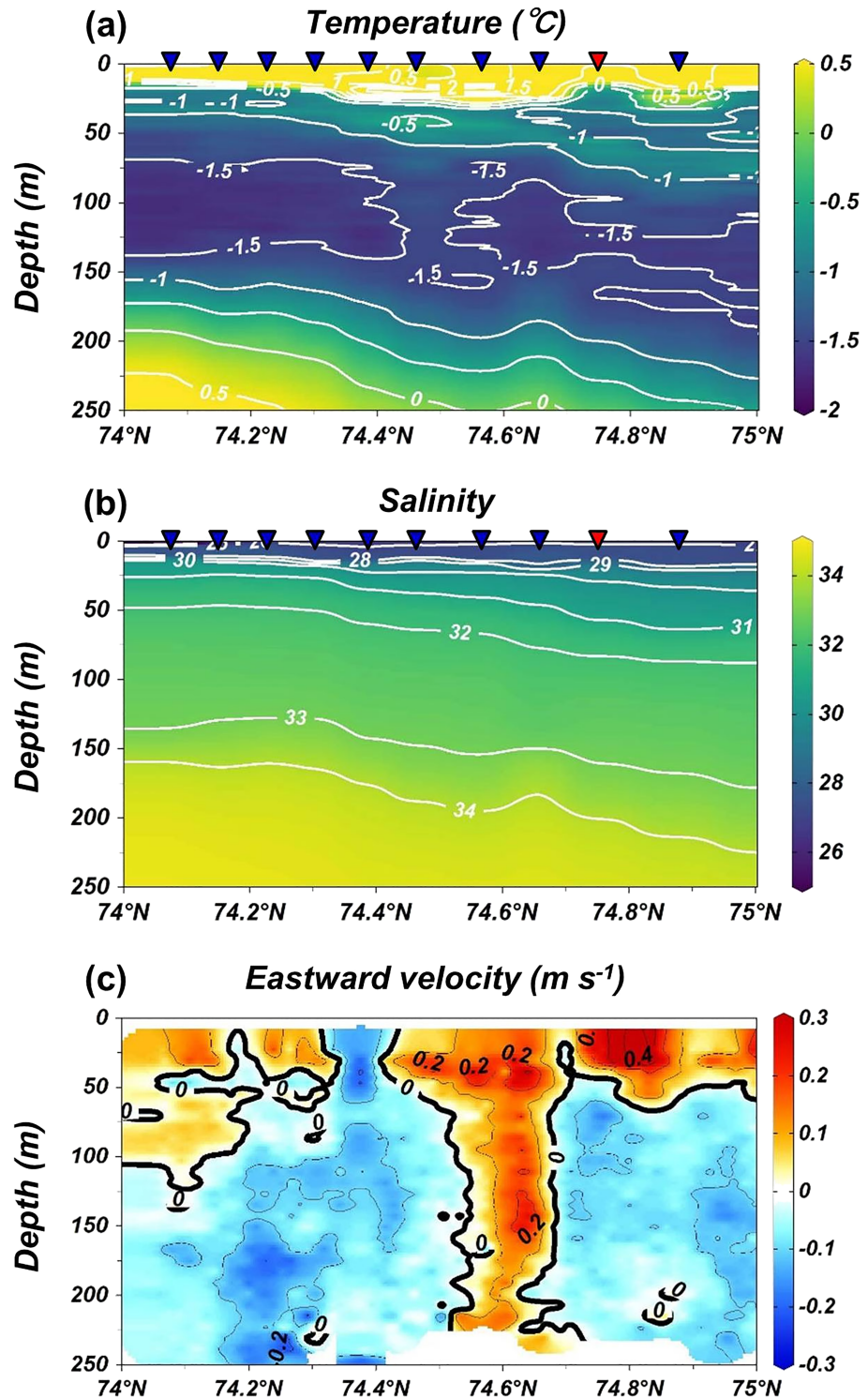
Figure 7. Vertical sections of (a) temperature (°C), (b) salinity, and (c) eastward velocity (m s^{-1}) across the FPO site on 5–6 September. The temperature and salinity data were obtained through expendable CTD (XCTD) surveys and the velocity was measured with a shipboard acoustic Doppler current profiler (ADCP). The survey line is part of the line shown in Figure 2 within the red rectangle, over a latitudinal range of 74°N to 75°N. In (a) and (b), blue inverted triangles at the top of each panel indicate the XCTD stations and the red inverted triangle represents the FPO site. In (c), ADCP data were obtained continuously along the survey line.
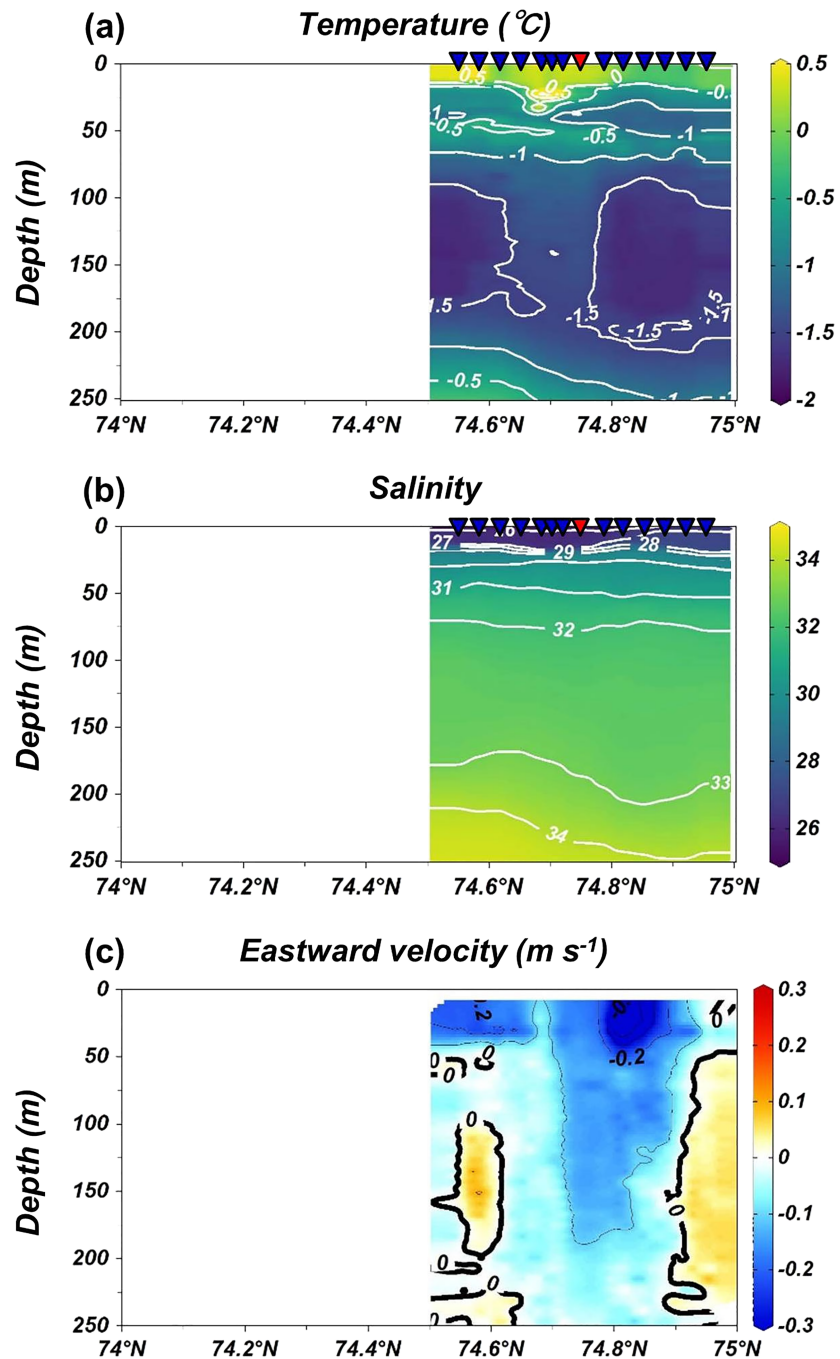
Figure 8. Vertical sections of (a) temperature (°C), (b) salinity, and (c) eastward velocity (m/s) across the FPO site on 18 September. The temperature and salinity data were obtained through XCTD surveys, and the velocity was measured with a shipboard ADCP. The survey line is part of the line shown in Figure 2 within the red rectangle, over a latitudinal range of 74.5°N to 75°N. In (a) and (b), blue inverted triangles at the top of each panel indicate XCTD stations and the red inverted triangle represents the FPO site. In (c), ADCP data were obtained continuously along the survey line.

(Figure 5c). These changes in surface water characteristics occurred on 17 September. On 14–21 September, we observed strong easterly winds (>8 m/s; Figure 4a). The zonal component of wind-driven currents in the surface layer around the FPO site was westward on 18 September (Figure 8c), and the subsurface current direction (~23 m) at the FPO site was northwestward (302°, not shown). Therefore, the northwestward advection of freshwater with relatively high chlorophyll *a* likely replaced the Term-II surface water with Term-III surface water. In the Canada Basin east of the FPO site, a large amount of freshwater accumulates

within the Beaufort Gyre (Proshutinsky et al., 2009; Wang et al., 2018). At the southern rim of the Beaufort Gyre, the surface layer seems largely influenced by high chlorophyll a water from the Chukchi Sea (e.g., Figures 2b and 2d in Nishino, Kikuchi, et al., 2011). In addition, a deep chlorophyll a maximum, which is likely found in the interior of the Beaufort Gyre, seems to extend to the southern rim of the gyre (Figure 2d in Nishino, Kikuchi, et al., 2011). Thus, two peaks of high chlorophyll a concentrations would have formed at the southern rim of the Beaufort Gyre, where the freshwater content was likely high. The water with a high freshwater content and two chlorophyll a peaks may have been transported to the FPO site during term-III by the northwestward flowing southern branch of the Beaufort Gyre.

4.2. Influence of Strong Wind Events on Ocean Characteristics

We observed several strong wind events during the FPO period, including an extended event between 14 and 21 September, when strong easterly winds blew over the FPO site, with wind speeds exceeding 12 m/s on 18–19 September (Figure 4a). During this event, significant turbulent mixing was observed in the ocean surface layer in response to the strong winds, but this mixing did not break through the seasonal pycnocline at ~20 m even during the strongest winds on 18–19 September (Figure 4b). This is consistent with previous studies by Randelhoff et al. (2014, 2017), who reported a rapid attenuation in the turbulent mixing at the seasonal pycnocline. On the other hand, strong mixing was observed down to depths of 20–30 m below the seasonal pycnocline on 11–12 September, despite the wind being calm. Based on the findings of Kawaguchi et al. (2016), this strong mixing was associated with internal waves that resulted from the passage of an anticyclonic cold-core eddy through the FPO site. In addition, Kawaguchi et al. (2016) suggested that temporal changes in wind direction at the beginning of the FPO could drive inertial motions, giving rise to turbulent internal waves at the seasonal pycnocline, as indicated by high ε compared with that at the seasonal pycnocline during the long period of continuous easterly winds.

Winds and eddies can cause significant turbulent mixing above and/or at the seasonal pycnocline, but the depth of the seasonal pycnocline (~20 m) was much shallower than that of the nutricline, which was ~60 m in the Canada Basin (Figure 6a). Thus, the mixing described above could not have contributed to nutrient fluxes across the nutricline or phytoplankton biomass (chlorophyll a) in the euphotic zone (~60 m; Brown et al., 2015). Randelhoff and Guthrie (2016) estimated that the nitrate flux across the nutricline in the Canada Basin was equivalent to 4.0×10^{-1} g C·m^{-2}·year^{-1} (carbon flux), which corresponds to 1.4×10^{-2} mmol N·m^{-2}·day^{-1} using the Redfield ratio (C:N = 106:16; Redfield et al., 1963). This nitrate flux was much smaller than the flux during a strong wind event in the Chukchi Sea (3.5 mmol N·m^{-2}·day^{-1}; Nishino et al., 2015) that resulted in increased phytoplankton production and biomass. The phytoplankton in the Chukchi Sea would be susceptible to wind forcing because of the shallow nutricline (~20 m). By contrast, the phytoplankton distribution in the present study was not related to wind forcing, but rather to the advection of water, as described in section 4.1. On the other hand, Kawaguchi et al. (2016) found that internal wave propagation caused by an anticyclonic cold-core eddy enhanced turbulent mixing in the lower halocline layer (200–250 m). However, this layer was much deeper than the euphotic zone, and thus, its mixing would not have influenced the phytoplankton distribution.

4.3. Characteristics of the Shallower Subsurface Chlorophyll a Maximum

In the Canada Basin, a subsurface chlorophyll a maximum generally develops at a depth of ~60 m, which corresponds to the deeper subsurface chlorophyll a maximum observed in the present study. This maximum has been well studied, including in terms of its distribution and seasonal dynamics (Brown et al., 2015; Carmack et al., 2004; Tremblay et al., 2008), biogeochemical significance (Martin et al., 2010), interannual changes in depth (McLaughlin & Carmack, 2010), and future projections (Steiner et al., 2016). However, the shallower subsurface chlorophyll a maximum at ~20 m has not been well studied to date. Therefore, we focus on this chlorophyll a maximum in this subsection, examining its characteristics and their implications for the Arctic marine ecosystem.

Figures 9a–9d show scatter plots of temperature, chlorophyll a, ammonium, and apparent oxygen utilization (AOU), respectively, with respect to depth during the FPO period. The red profile in each scatter plot shows the data obtained on 10 September, when an anomalously high ammonium concentration and abundant large-sized phytoplankton biomass were observed at 20 m (Figures 6b and 6c, respectively). At that time, the vertical maxima of both temperature and chlorophyll a occurred at 20 m, with the nearly highest
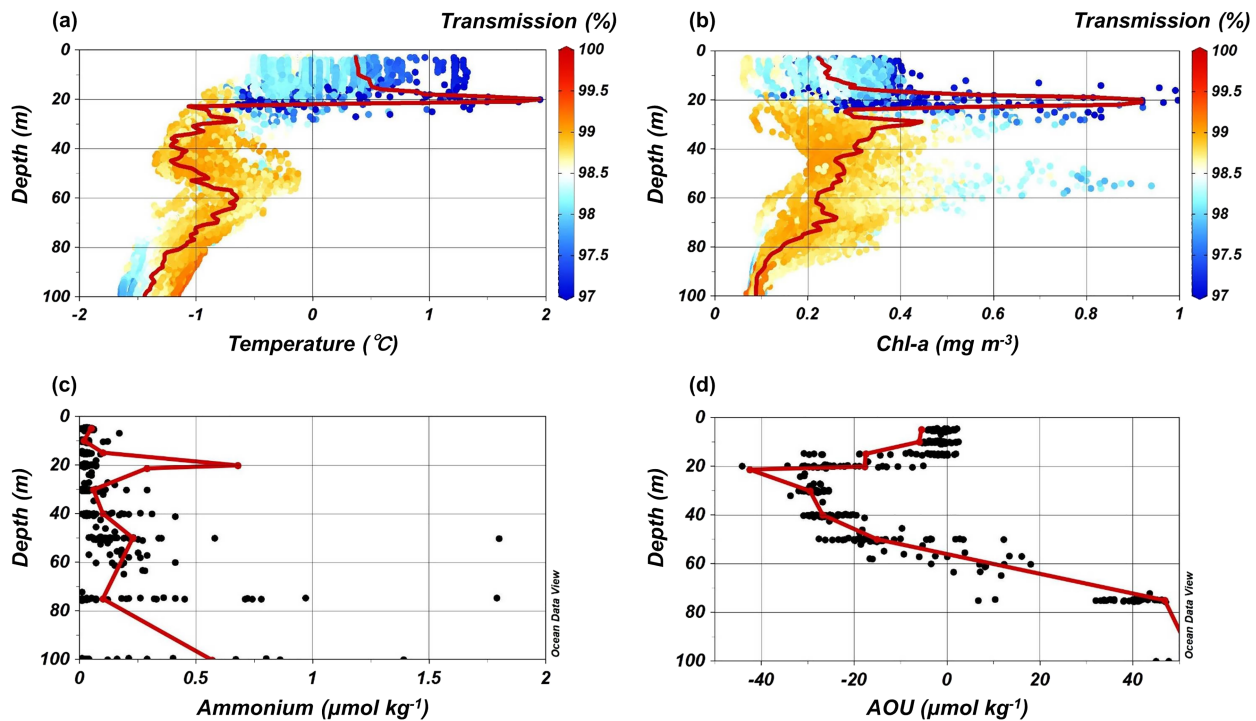
Figure 9. Scatter plots of (a) temperature (°C), (b) chlorophyll a (fluorescence) (mg m^{-3}), (c) ammonium (μmol/kg), and (d) apparent oxygen utilization (AOU) (μmol kg^{-1}) with respect to depth during the FPO period. The red profile in each panel shows data obtained on 10 September. In (a) and (b), colors indicate transmission (%), and all data were obtained using sensors attached to the CTD profiler. In (c) and (d), the data were obtained through water sampling.

values observed during the FPO period (Figures 9a and 9b, respectively). The transmission there was extremely low (indicated by dark blue in Figures 9a and 9b), and its minimum appeared at 18 m (not shown). The chlorophyll a maximum at 20 m corresponded to the ammonium maximum and AOU minimum (Figures 9c and 9d, respectively). The AOU had negative values around the chlorophyll a maximum, suggesting oxygen production there, likely due to photosynthesis. The high rate of photosynthesis needed to drive the AOU minimum was likely sustained by the high concentration of ammonium at its maximum depth (20 m), despite nitrate depletion.

The AOU at 20 m on 10 September (−42.5 μmol/kg) was 12.5 μmol/kg lower than what was usually observed at that depth (−30 μmol/kg on average; Figure 9d). This implies that the water at 20 m on 10 September contained anomalous oxygen (12.5 μmol/kg) that was associated with significant photosynthesis at the chlorophyll a maximum. Based on the Redfield ratio (N:O$_2$ = 16:−138; Redfield et al., 1963), the anomalous oxygen corresponded to 1.45 μmol/kg ammonium (N) used for photosynthesis. The observed (residual) ammonium concentration at 20 m on 10 September was 0.68 μmol/kg, and thus, the water there should have originally contained an ammonium concentration of ~2 μmol/kg. Such high ammonium concentrations are generally not observed in the Canada Basin (Nishino et al., 2005, 2008).

One conceivable ammonium source may be warm-core eddies carrying nutrients, including ammonium, from the Chukchi Sea into the Canada Basin (Nishino et al., 2018; Nishino, Itoh, et al., 2011). However, the eddies will not always contain ammonium because the ammonium is likely consumed by phytoplankton during its transport from the Chukchi Sea to the FPO site. Shiozaki et al. (2019) estimated that the time scale of ammonium consumption was on the order of 10 days in the southern Canada Basin. Assuming that the warm-core eddies were formed in August near Point Barrow, Alaska (Watanabe & Hasumi, 2009), the ammonium in the eddies would have been largely consumed before our observations at the FPO site in mid-September. In fact, on 18 September, when a warm-core eddy occupied the FPO site (Figure 8), the ammonium concentration in the eddy (~25 m) was almost 0 (Figure 6b). Nevertheless, we found a prominent chlorophyll a maximum at 25 m (shallower subsurface chlorophyll a maximum) on 18 September (Figure 5c) and abundant large-sized phytoplankton biomass (Figure 6c), similar to those at 20 m on 10 September. As mentioned above, the ammonium concentration at 20 m on 10 September was 0.68 μmol/

kg, and the water should have originally contained ~2 μmol/kg ammonium. In other words, if a warm-core eddy originally contained ~2 μmol/kg ammonium, it would be possible for it to reach the FPO site with a detectable concentration (0.68 μmol/kg) of ammonium. However, even in a warm-core eddy found near its formation site over the Chukchi shelf slope off the coast of Alaska, the ammonium concentration was ~0.9 μmol/kg at the depth of the temperature maximum (Nishino et al., 2018). This is about half of the ammonium concentration (~2 μmol/kg) required to sustain the photosynthesis that caused the anomalous AOU minimum at 20 m on 10 September at the FPO site. Although warm-core eddies might be an important ammonium source, such eddies alone cannot fully explain the increased photosynthesis. Thus, other ammonium sources were necessary.

Another plausible source is regenerated ammonium at the seasonal pycnocline. Transmission was extremely low at the seasonal pycnocline (~20 m) during Term-I and Term-III (Figure 5d), suggesting the accumulation of particles on the interface of the density discontinuity. Yamada et al. (2015) also observed particle accumulation on the pycnocline using laser in situ scattering and transmissometry in the Chukchi Sea and the Canada Basin. Some of the accumulated particles were particulate organic matter (POM), and in the Canada Basin (FPO site), POM may have been derived not only from the surface layer but also from the Chukchi Sea (Bates et al., 2005; Yamada et al., 2015). The accumulated POM at the FPO site seasonal pycnocline would have decomposed, regenerating ammonium. This regenerated ammonium could be generally consumed for photosynthesis, leading to an observed ammonium concentration of almost zero at the seasonal pycnocline, except in water masses that had originally contained a large amount of ammonium, such as the ammonium maximum water found at 20 m on 10 September.

4.4. Future Phytoplankton Changes

The FPO was conducted during the fall season, when the ocean had started cooling but had not frozen up yet. During the FPO period (~3 weeks), the surface water characteristics, including the chlorophyll *a* concentration, were changed temporally, mainly due to the replacement of water masses rather than seasonal forcing such as ocean cooling. The temporal change in the shallower subsurface chlorophyll *a* maximum was more complicated. The chlorophyll *a* concentrations there were likely controlled by warm-core eddies and POM accumulations at the seasonal pycnocline, both of which are sources of ammonium, and that had changed rapidly compared with the time scale of the changes in the surface water chlorophyll *a* concentration. In this subsection, we discuss phytoplankton changes in a time scale of climate changes such as sea ice reduction while referring to the results of the previous studies.

In the present study, no phytoplankton responses to strong wind events were detected at the FPO site in the Canada Basin due to the deep nutricline in comparison with the seasonal pycnocline, where the turbulent mixing was largely attenuated. This is consistent with the report of Lincoln et al. (2016), who found that the stratification in the Canada Basin suppressed the turbulent mixing at intermediate depths and isolated the Pacific-origin (nutrient-rich) water from the sea surface. This strong suppression of turbulent mixing occurred even in the unusually ice-free and stormy summer of 2012 in the Canada Basin. In addition, based on numerical models, the nutricline and subsurface chlorophyll *a* maximum in the Canada Basin will continue to deepen in future climate scenarios (Steiner et al., 2016). Thus, the nutrient and phytoplankton distributions in the Canada Basin are likely to be unresponsive to strong wind events in the future, as in the present study.

In contrast to the Canada Basin, nutriclines in the southern Makarov Basin and in the central Arctic Ocean are shallow due to the supply of nutrient-rich waters from the East Siberian Sea, which are less saline than the nutrient-rich Pacific-origin water (Alkire et al., 2019; Nishino et al., 2013), in addition to a thin layer of freshwater above the nutricline. In particular, the nutricline in the southern Makarov Basin was shallower in the late 2000s than in the early 2000s (Nishino et al., 2013). In the late 2000s, a delayed fall freeze-up in the eastern East Siberian Sea would have enhanced the water cooling and convection that entrained nutrients from the shelf bottom to the water column, and such nutrient-rich shelf water was spread just below the surface mixed layer in the southern Makarov Basin, resulting in the coinciding seasonal pycnocline and nutricline (Figures 2j and 3d in Nishino et al., 2013). Although we do not have data on the turbulent mixing in the southern Makarov Basin, the coinciding seasonal pycnocline and nutricline in this region may induce increases in nutrient fluxes and phytoplankton biomass during strong wind events, as observed in the Chukchi Sea (Nishino et al., 2015). If the sea ice disappears over a greater area in the East Siberian Sea

until the fall freeze-up season in the future, a greater volume of nutrient-rich shelf water could spread into the Makarov Basin, which may cause the marine ecosystem there to become responsive to wind forcing. However, future accelerated sea ice melt may strengthen stratification and suppress nutrient fluxes in the central Arctic Ocean (Randelhoff & Guthrie, 2016).

Sea ice loss caused by Arctic warming may also increase the number, volume, and lifespan of eddies in the Canada Basin (Kawaguchi et al., 2012; Watanabe et al., 2012, 2014). The present study indicates the importance of warm-core eddies to the development of a prominent chlorophyll a maximum at the seasonal pycnocline (shallower subsurface chlorophyll a maximum) in the Canada Basin. Therefore, if the eddy number increases due to future sea ice loss, areas with prominent chlorophyll a maxima and abundant large-sized phytoplankton would increase. Furthermore, if the eddy lifespan increases in the future, the rotation velocities of eddies would not be attenuated even in areas far downstream of the eddy-formation region over the Chukchi shelf slope (Pickart et al., 2005; Spall et al., 2008) and Barrow Canyon off the coast of Alaska (Watanabe & Hasumi, 2009). In this case, as described by Nishino et al. (2018), velocity shear within the eddy could cause vertical mixing, driving upward nutrient fluxes, and the resultant flourishing of phytoplankton even downstream of the eddy, such as at the FPO site. Future warming of warm-core eddies may enhance double-diffusive mixing in the interleaving structures at the rim of such eddies, resulting in increases in upward nutrient fluxes and phytoplankton biomass (Nishino et al., 2018). Such enhanced eddy activity could increase the transport of POM from the Chukchi Sea into the Canada Basin (Watanabe et al., 2014), and this transported POM might accumulate on the seasonal pycnocline in the Canada Basin. Thus, warm-core eddies may play a greater role in chlorophyll a distribution and the marine ecosystem in the future.

5. Summary

We examined oceanic and biological responses to wind forcing during strong wind events in fall 2014 at an FPO station in the NAP of the Canada Basin (74.75°N, 162°W). At the FPO station, observations were collected at high temporal resolution, including ocean microstructure (every 6 hr), CTD (every 6 hr), and water sampling (every 12 hr), along with ADCP and XCTD surveys. We detected internal wave propagation, eddy passage, and water mass changes that were assumed to influence the nutrient and phytoplankton distributions in the Canada Basin.

The 3-week observation period included two strong wind events (6–9 and 14–21 September; Figure 4a); during both events, the resultant enhanced mixing was sharply attenuated below the seasonal pycnocline at ~20 m (Figure 4b). However, strong mixing (11–12 September) associated with internal waves resulting from the passage of an anticyclonic cold-core eddy was found even below the seasonal pycnocline to depths of 20–30 m.

The depths at which significant wind- and eddy-induced mixing were observed were much shallower than the nutricline (~60 m; Figure 6a). Such mixing does not drive vertical nutrient fluxes and thus did not influence the phytoplankton (chlorophyll a) distribution in the surface layer (Figure 5c). The chlorophyll a concentration in the surface layer was determined by the advection of water masses, such as the intrusion of basin-side water on 11 September (Figures 2b–2d) and the arrival of high-f_{OF} water on 17 September (Figure 6d). Prominent subsurface chlorophyll a maxima were found at the seasonal pycnocline on 10 and 18 September (Figure 5c) and large-sized phytoplankton flourished in the chlorophyll a maxima on these dates (Figure 6c). The prominent subsurface chlorophyll a maximum and abundant large-sized phytoplankton biomass were likely carried to the FPO site by a warm-core eddy (Figure 8).

The prominent subsurface chlorophyll a maximum on 10 September was accompanied by an ammonium maximum (Figures 6b and 9c) and AOU minimum (Figure 9d). Thus, phytoplankton biomass may have been sustained by the high concentration of ammonium. The AOU was lower than usual in this sample, implying that the phytoplankton were not carcasses carried by the warm-core eddy but were organisms living within the eddy despite the great distance from nutrient-rich shelf areas. One nutrient source for the phytoplankton was the eddy, which contained a large amount of ammonium. Another possible source was regenerated ammonium at the seasonal pycnocline, where POM accumulated and decomposed, producing ammonium.

In future research, we should extend the FPO approach to other Arctic basins, for example, the southern Makarov Basin, where the nutricline may be shoaling due to sea ice loss. If the nutrient and phytoplankton distributions are influenced by strong wind events in other Arctic basins, further studies are needed, including observations of higher trophic levels in the marine ecosystem, CO_2 exchange between the atmosphere and ocean, and carbon transport to the sediment. Carrying out FPO studies every few years would allow monitoring of eddy activity and its impact on the marine ecosystem, which is expected to increase with future sea ice loss.

References

Aagaard, K., Coachman, L. K., & Carmack, E. (1981). On the halocline of the Arctic Ocean. *Deep Sea Research Part A: Oceanographic Research Papers*, *28*, 529–545. https://doi.org/10.1016/0198-0149(81)90115-1

Aguilar-Islas, A. M., Rember, R., Nishino, S., Kikuchi, T., & Itoh, M. (2013). Partitioning and lateral transport of iron to the Canada Basin. *Polar Science*, *7*(2), 82–99. https://doi.org/10.1016/j.polar.2012.11.001

Alkire, M. B., Rember, R., & Polyakov, I. (2019). Discrepancy in the identification of the Atlantic/Pacific front in the central Arctic Ocean: NO versus nutrient relationships. *Geophysical Research Letters*, *46*, 3843–3852. https://doi.org/10.1029/2018GL081837

Aoyama, M., & Hydes, D. J. (2010). How do we improve the comparability of nutrient measurements? In M. Aoyama, A. G. Dickson, D. J. Hydes, A. Murata, J. R. Oh, P. Roose, & E. M. S. Woodward (Eds.), *Comparability of nutrients in the world's ocean*, (pp. 1–10). Tsukuba, Japan: Mother Tank.

Ardyna, M., Babin, M., Gosselin, M., Devred, E., Rainville, L., & Tremblay, J.-É. (2014). Recent Arctic Ocean sea ice loss triggers novel fall phytoplankton blooms. *Geophysical Research Letters*, *41*, 6207–6212. https://doi.org/10.1002/2014GL061047

Bates, N. R., Hansell, D. A., Moran, S. B., & Codispoti, L. A. (2005). Seasonal and spatial distribution of particulate organic matter (POM) in the Chukchi and Beaufort Seas. *Deep Sea Research Part II: Topical Studies in Oceanography*, *52*, 3324–3343. https://doi.org/10.1016/j.dsr2.2005.10.003

Brown, Z. W., Lowry, K. E., Palmer, M. A., van Dijken, G. L., Mills, M. M., Pickart, R. S., & Arrigo, K. R. (2015). Characterizing the subsurface chlorophyll *a* maximum in the Chukchi Sea and Canada Basin. *Deep Sea Research Part II: Topical Studies in Oceanography*, *118*(Part A), 88–104. https://doi.org/10.1016/j.dsr2.2015.02.010

Carmack, E. C., Macdonald, R. W., & Jasper, S. (2004). Phytoplankton productivity on the Canadian Shelf of the Beaufort Sea. *Marine Ecology Progress Series*, *277*, 37–50. https://doi.org/10.3354/meps277037

Coachman, L. K., Aagaard, K., & Tripp, R. B. (1975). *Bering Strait: The regional physical oceanography*. Seattle, WA: University of Washington Press.

Coachman, L. K., & Barnes, C. A. (1961). The contribution of Bering Sea water to the Arctic Ocean. *Arctic*, *14*, 147–161. https://doi.org/10.14430/arctic3670

Codispoti, L. A., Flagg, C., Kelly, V., & Swift, J. H. (2005). Hydrographic conditions during the 2002 SBI process experiments. *Deep Sea Research Part II: Topical Studies in Oceanography*, *52*, 3199–3226. https://doi.org/10.1016/j.dsr2.2005.10.007

Comiso, J. C., Meier, W. N., & Gersten, R. (2017). Variability and trends in the Arctic Sea ice cover: Results from different techniques. *Journal of Geophysical Research: Oceans*, *122*, 6883–6900. https://doi.org/10.1002/2017JC012768

Coupel, P., Ruiz-Pino, D., Sicre, M. A., Chen, J. F., Lee, S. H., Schiffrine, N., et al. (2015). The impact of freshening on phytoplankton production in the Pacific Arctic Ocean. *Progress in Oceanography*, *131*, 113–125. https://doi.org/10.1016/j.pocean.2014.12.003

Dickson, A. G. (1996). Determination of dissolved oxygen in sea water by Winkler titration. *WOCE Operations Manual* (Volume 3, Section 3.1, Part 3.1.3 WHP Operations and Methods, WHP Office Report WHPO 91-1, WOCE Report No. 68/91, Nov. 1994, Revision 1, pp. 1–13). Woods Hole, MA. Retrieved from https://www.nodc.noaa.gov/woce/woce_v3/wocedata_1/whp/manuals/pdf/91_1/dickson2.pdf

Fujiwara, A., Nishino, S., Matsuno, K., Onodera, J., Kawaguchi, Y., Hirawake, T., et al. (2018). Changes in phytoplankton community structure during wind-induced fall bloom on the central Chukchi shelf. *Polar Biology*, *41*, 1279–1295. https://doi.org/10.1007/s00300-018-2284-7

Hydes, D. J., Aoyama, M., Aminot, A., Bakker, K., Becker, S., Coverly, S., et al. (2010). Determination of dissolved nutrients (N, P, Si) in seawater with high precision and inter-comparability using gas-segmented continuous flow analysers. In E. M. Hood, C. L. Sabine, & B. M. Sloyan (Eds.), *The GO-SHIP Repeat Hydrography Manual: A Collection of Expert Reports and Guidelines* (IOCCP Report Number 14, ICPO Publication Series Number 134, pp. 1–87). Paris, France: UNESCO-IOC. Retrieved from http://www.go-ship.org/HydroMan.html, http://www.go-ship.org/Manual/Hydes_et_al_Nutrients.pdf

Inoue, J. (2014). *R/V Mirai Cruise Report MR14-05*. Yokosuka, Japan: JAMSTEC. Retrieved from. http://www.godac.jamstec.go.jp/darwin/datatree/e

Inoue, J., Sato, K., & Oshima, K. (2018). Comparison of the Arctic tropospheric structures from the ERA-Interim reanalysis with in situ observations. *Okhotsk Sea and Polar Oceans Research*, *2*, 7–12.

Jackson, J. M., Carmack, E. C., McLaughlin, F. A., Allen, S. E., & Ingram, R. G. (2010). Identification, characterization, and change of the near-surface temperature maximum in the Canada Basin, 1993–2008. *Journal of Geophysical Research*, *115*, C05021. https://doi.org/10.1029/2009JC005265

Kawaguchi, Y., Itoh, M., Fukamachi, Y., Moriya, E., Onodera, J., Kikuchi, T., & Harada, N. (2019). Year-round observations of sea-ice drift and near-inertial internal waves in the Northwind Abyssal Plain, Arctic Ocean. *Polar Science*, *21*, 212–223. https://doi.org/10.1016/j.polar.2019.01.004

Kawaguchi, Y., Itoh, M., & Nishino, S. (2012). A detailed survey of a large baroclinic eddy with extremely high temperature in the western Canada Basin. *Deep Sea Research Part I: Oceanographic Research Papers*, *66*, 90–102. https://doi.org/10.1016/j.dsr.2012.04.006

Kawaguchi, Y., Nishino, S., & Inoue, J. (2015). Fixed-point observation of mixed layer evolution in the seasonally ice-free Chukchi Sea: Turbulent mixing due to gale winds and internal gravity waves. *Journal of Physical Oceanography*, *45*, 836–853. https://doi.org/10.1175/JPO-D-14-0149.1

Kawaguchi, Y., Nishino, S., Inoue, J., Maeno, K., Takeda, H., & Oshima, K. (2016). Enhanced diapycnal mixing due to near-inertial internal waves propagating through an anticyclonic eddy in the ice-free Chukchi Plateau. *Journal of Physical Oceanography*, *46*, 2457–2481. https://doi.org/10.1175/JPO-D-15-0150.1

Kawano, T. (2010). Method for salinity (conductivity ratio) measurement. In E. M. Hood, C. L. Sabine, & B. M. Sloyan (Eds.), *The GO-SHIP repeat hydrography manual: A collection of expert reports and guidelines* (IOCCP Report Number 14, ICPO Publication Series Number 134, (pp. 1–13). Paris, France: UNESCO-IOC. Retrieved from. http://www.go-ship/HydroMan.html, http://www.go-ship.org/Manual/Kawano_Salinity.pdf

Killworth, P. D., & Smith, J. M. (1984). A one-and-a-half dimensional model for the Arctic halocline. *Deep Sea Research Part A: Oceanographic Research Papers*, *31*, 271–293. https://doi.org/10.1016/0198-0149(84)90105-5

Li, W. K. W., McLaughlin, F. A., Lovejoy, C., & Carmack, E. C. (2009). Smallest algae thrive as the Arctic Ocean freshens. *Science*, *326*(5952), 539. https://doi.org/10.1126/science.1179798

Lincoln, B. J., Rippeth, T. P., Lenn, Y.-D., Timmermans, M. L., Williams, W. J., & Bacon, S. (2016). Wind-driven mixing at intermediate depths in an ice-free Arctic Ocean. *Geophysical Research Letters*, *43*, 9749–9756. https://doi.org/10.1002/2016GL070454

Loeng, H., Brander, K., Carmack, E., Denisenko, S., Drinkwater, K., Hansen, B., et al. (2005). Chapter 9: Marine systems. In C. Symon, L. Arris, & B. Heal (Eds.), *Arctic Climate Impact Assessment, ACIA overview report*, (pp. 453–538). New York, NY: Cambridge University Press. Retrieved from. https://www.amap.no/documents/download/1090/inline

Martin, J., Tremblay, J.-É., Gagnon, J., Tremblay, G., Lapoussière, A., Jose, C., et al. (2010). Prevalence, structure and properties of sub-surface chlorophyll maxima in Canadian Arctic water. *Marine Ecology Progress Series*, *412*, 69–84. https://doi.org/10.3354/meps08666

Matsuno, K., Yamaguchi, A., Nishino, S., Inoue, J., & Kikuchi, T. (2015). Short-term changes in the mesozooplankton community and copepod gut pigment in the Chukchi Sea in autumn: reflections of a strong wind event. *Biogeosciences*, *12*, 4005–4015. https://doi.org/10.5194/bg-12-4005-2015

McCabe, G. J., Clarc, M. P., & Serreze, M. C. (2001). Trends in Northern Hemisphere surface cyclone frequency and intensity. *Journal of Climate*, *14*, 2763–2768. https://doi.org/10.1175/1520-0442(2001)014<2763:TINHSC>2.0.CO;2

McLaughlin, F. A., & Carmack, E. C. (2010). Deepening of the nutricline and chlorophyll maximum in the Canada Basin interior, 2003-2009. *Geophysical Research Letters*, *37*, L24602. https://doi.org/10.1029/2010GL045459

McPhee, M. G., Stanton, T. P., Morison, J. H., & Martinson, D. G. (1998). Freshening of the upper ocean in the Arctic: Is perennial sea ice disappearing? *Geophysical Research Letters*, *25*, 1729–1732. https://doi.org/10.1029/98GL00933

Nishino, S., Itoh, M., Kawaguchi, Y., Kikuchi, T., & Aoyama, M. (2011). Impact of an unusually large warm-core eddy on distributions of nutrients and phytoplankton in the southwestern Canada Basin during late summer/early fall 2010. *Geophysical Research Letters*, *38*, L16602. https://doi.org/10.1029/2011GL047885

Nishino, S., Itoh, M., Williams, W. J., & Semiletov, I. (2013). Shoaling of the nutricline with an increase in near-freezing temperature water in the Makarov Basin. *Journal of Geophysical Research: Oceans*, *118*, 635–649. https://doi.org/10.1029/2012JC008234

Nishino, S., Kawaguchi, Y., Fujiwara, A., Shiozaki, T., Aoyama, M., Harada, N., & Kikuchi, T. (2018). Biogeochemical anatomy of a cyclonic warm-core eddy in the Arctic Ocean. *Geophysical Research Letters*, *45*, 11,284–11,292. https://doi.org/10.1029/2018GL079659

Nishino, S., Kawaguchi, Y., Inoue, J., Hirawake, T., Fujiwara, A., Futsuki, R., et al. (2015). Nutrient supply and biological response to wind-induced mixing, inertial motion, internal waves, and currents in the northern Chukchi Sea. *Journal of Geophysical Research: Oceans*, *120*, 1975–1992. https://doi.org/10.1002/2014JC010407

Nishino, S., Kikuchi, T., Yamamoto-Kawai, M., Kawaguchi, Y., Hirawake, T., & Itoh, M. (2011). Enhancement/reduction of biological pump depends on ocean circulation in the sea-ice reduction regions of the Arctic Ocean. *Journal of Oceanography*, *67*, 305–314. https://doi.org/10.1007/s10872-011-0030-7

Nishino, S., Shimada, K., & Itoh, M. (2005). Use of ammonium and other nitrogen tracers to investigate the spreading of shelf waters in the western Arctic halocline. *Journal of Geophysical Research*, *110*, C10005. https://doi.org/10.1029/2003JC002118

Nishino, S., Shimada, K., Itoh, M., Yamamoto-Kawai, M., & Chiba, S. (2008). East-west differences in water mass, nutrient, and chlorophyll *a* distributions in the sea-ice reduction region of the western Arctic Ocean. *Journal of Geophysical Research*, *113*, C00A01. https://doi.org/10.1029/2007JC004666

Orlanski, I. (1998). Poleward deflection of storm tracks. *Journal of the Atmospheric Sciences*, *55*, 2577–2602. https://doi.org/10.1175/1520-0469(1998)055<2577:PDOST>2.0.CO;2

Pickart, R. S., Weingartner, T. J., Pratt, L. J., Zimmermann, S., & Torres, D. J. (2005). Flow of winter-transformed Pacific water into the Western Arctic. *Deep Sea Research Part II: Topical Studies in Oceanography*, *52*, 3175–3198. https://doi.org/10.1016/j.dsr2.2005.10.009

Proshutinsky, A., Krishfield, R., Timmermans, M.-L., Toole, J., Carmack, E., McLaughlin, F., et al. (2009). Beaufort Gyre freshwater reservoir: State and variability from observations. *Journal of Geophysical Research*, *114*, C00A10. https://doi.org/10.1029/2008JC005104

Rainville, L., Lee, C. M., & Woodgate, R. A. (2011). Impact of wind-driven mixing in the Arctic Ocean. *Oceanography*, *24*, 136–145. https://doi.org/10.5670/oceanog.2011.65

Rainville, L., & Woodgate, R. A. (2009). Observations of internal wave generation in the seasonally ice-free Arctic. *Geophysical Research Letters*, *36*, L23604. https://doi.org/10.1029/2009GL041291

Randelhoff, A., Fer, I., & Sundfjord, A. (2017). Turbulent upper-ocean mixing affected by meltwater layers during Arctic summer. *Journal of Physical Oceanography*, *47*, 835–853. https://doi.org/10.1175/jpo-d-16-0200.1

Randelhoff, A., Fer, I., Sundfjord, A., Tremblay, J.-E., & Reigstad, M. (2016). Vertical fluxes of nitrate in the seasonal nitracline of the Atlantic sector of the Arctic Ocean. *Journal of Geophysical Research: Oceans*, *121*, 5282–5295. https://doi.org/10.1002/2016JC011779

Randelhoff, A., & Guthrie, J. D. (2016). Regional patterns in current and future export production in the central Arctic Ocean quantified from nitrate fluxes. *Geophysical Research Letters*, *43*, 8600–8608. https://doi.org/10.1002/2016GL070252

Randelhoff, A., Sundfjord, A., & Renner, A. H. H. (2014). Effects of a shallow pycnocline and surface meltwater on sea ice-ocean drag and turbulent heat flux. *Journal of Physical Oceanography*, *44*, 2176–2190. https://doi.org/10.1175/jpo-d-13-0231.1

Redfield, A. C., Ketchum, B. H., & Richards, F. A. (1963). The influence of organisms on the composition of seawater. In M. N. Hill (Ed.), *The Sea*, (Vol. 2, pp. 26–77). New York, NY: Wiley.

Sato, K., Aoyama, M., & Becker, S. (2010). Reference materials for nutrients in seawater as calibration standard solution to keep comparability for several cruises in the world ocean in 2000s. In M. Aoyama, A. G. Dickson, D. J. Hydes, A. Murata, J. R. Oh, P. Roose, & E. M. S. Woodward (Eds.), *Comparability of nutrients in the world's ocean*, (pp. 43–56). Tsukuba, Japan: Mother Tank.

Schlitzer, R. (2018). *Ocean Data View*. Bremerhaven, Germany: Alfred-Wegener-Institut. Retrieved from. https://odv.awi.de

Sepp, M., & Jaagus, J. (2011). Changes in the activity and tracks of Arctic cyclones. *Climatic Change*, *105*, 577–595. https://doi.org/10.1007/s10584-010-9893-7

Serreze, M. C., Holland, M. M., & Stroeve, J. (2007). Perspectives on the Arctic's shrinking sea-ice cover. *Science*, *315*, 1533–1536. https://doi.org/10.1126/science.1139426

Serreze, M. C., Walsh, J. E., Chapin, S. F. III, Osterkamp, T., Dyurgerov, M., Romanovsky, V., et al. (2000). Observational evidence of recent change in the northern high-latitude environment. *Climatic Change*, *46*, 159–207. https://doi.org/10.1023/A:1005504031923

Shimada, K., Carmack, E. C., Hatakeyama, K., & Takizawa, T. (2001). Varieties of shallow temperature maximum waters in the western Canada Basin of the Arctic Ocean. *Geophysical Research Letters*, *28*, 3441–3444. https://doi.org/10.1029/2001GL013168

Shimada, K., Itoh, M., Nishino, S., McLaughlin, F., Carmack, E., & Proshutinsky, A. (2005). Halocline structure in the Canada Basin of the Arctic Ocean. *Geophysical Research Letters*, *32*, L03605. https://doi.org/10.1029/2004GL021358

Shiozaki, T., Ijichi, M., Fujiwara, A., Makabe, A., Nishino, S., Yoshikawa, C., & Harada, N. (2019). Factors regulating nitrification in the Arctic Ocean: Potential impact of sea ice reduction and ocean acidification. *Global Biogeochemical Cycles*, *33*, 1085–1099. https://doi.org/10.1029/2018GB006068

Spall, M. A., Pickart, R. S., Fratantoni, P., & Plueddemann, A. J. (2008). Western Arctic shelfbreak eddies: formation and transport. *Journal of Physical Oceanography*, *38*, 1644–1668. https://doi.org/10.1175/2007JPO3829.1

Steiner, N. S., Sou, T., Deal, C., Jackson, J. M., Jin, M., Popova, E., et al. (2016). The future of the subsurface chlorophyll-*a* maximum in the Canada Basin—A model intercomparison. *Journal of Geophysical Research: Oceans*, *121*, 387–409. https://doi.org/10.1002/2015JC011232

Stroeve, J., Kattsov, V., Barrett, A., Serreze, M., Pavlova, T., Holland, M., & Meier, W. N. (2012). Trends in Arctic sea ice extent from CMIP5, CMIP3 and observations. *Geophysical Research Letters*, *39*, L16502. https://doi.org/10.1029/2012GL052676

Tremblay, J.-É., Simpson, K., Martin, J., Miller, L., Gratton, Y., Barber, D., & Price, N. M. (2008). Vertical stability and the annual dynamics of nutrients and chlorophyll fluorescence in the coastal, southeast Beaufort Sea. *Journal of Geophysical Research*, *113*, C07S90. https://doi.org/10.1029/2007JC004547

Wang, Q., Wekerle, C., Danilov, S., Koldunov, N., Sidorenko, D., Sein, D., et al. (2018). Arctic sea ice decline significantly contributed to the unprecedented liquid freshwater accumulation in the Beaufort Gyre of the Arctic Ocean. *Geophysical Research Letters*, *45*, 4956–4964. https://doi.org/10.1029/2018GL077901

Watanabe, E., & Hasumi, H. (2009). Pacific water transport in the western Arctic Ocean simulated by an eddy-resolving coupled sea ice-ocean model. *Journal of Physical Oceanography*, *39*, 2194–2211. https://doi.org/10.1175/2009JPO4010.1

Watanabe, E., Kishi, M. J., Ishida, A., & Aita, M. N. (2012). Western Arctic primary productivity regulated by shelf-break warm eddies. *Journal of Oceanography*, *68*, 703–718. https://doi.org/10.1007/s10872-012-0128-6

Watanabe, E., Onodera, J., Harada, N., Honda, M. C., Kimoto, K., Kikuchi, T., et al. (2014). Enhanced role of eddies in the Arctic marine biological pump. *Nature Communications*, *5*, 3950. https://doi.org/10.1038/ncomms4950

Welschmeyer, N. A. (1994). Fluorometric analysis of chlorophyll *a* in the presence of chlorophyll *b* and pheopigments. *Limnology and Oceanography*, *39*, 1985–1992. https://doi.org/10.4319/lo.1994.39.8.1985

Wolk, F., Yamazaki, H., Seuront, L., & Lueck, R. G. (2002). A new free-fall profiler for measuring biophysical microstructure. *Journal of Atmospheric and Oceanic Technology*, *19*, 780–793. https://doi.org/10.1175/1520-0426(2002)019<0780:ANFFPF>2.0.CO;2

Yamada, Y., Fukuda, H., Uchimiya, M., Motegi, C., Nishino, S., Kikuchi, T., & Nagata, T. (2015). Localized accumulation and a shelf-basin gradient of particles in the Chukchi Sea and Canada Basin, western Arctic. *Journal of Geophysical Research: Oceans*, *120*, 4638–4653. https://doi.org/10.1002/2015JC010794

Yamamoto-Kawai, M., Tanaka, N., & Pivovarov, S. (2005). Freshwater and brine behaviors in the Arctic Ocean deduced from historical data of δ^{18}O and alkalinity (1929–2002 A.D.). *Journal of Geophysical Research*, *110*, C10003. https://doi.org/10.1029/2004JC002793

Yao, W., & Byrne, R. H. (1998). Simplified seawater alkalinity analysis: Use of linear array spectrometers. *Deep Sea Research Part I: Oceanographic Research Papers*, *45*, 1383–1392. https://doi.org/10.1016/S0967-0637(98)00018-1

Yokoi, N., Matsuno, K., Ichinomiya, M., Yamaguchi, A., Nishino, S., Onodera, J., et al. (2016). Short-term changes in a microplankton community in the Chukchi Sea during autumn: consequences of a strong wind event. *Biogeosciences*, *13*, 913–923. https://doi.org/10.5194/bg-13-913-2016

Yun, M. S., Kim, B. K., Joo, H. T., Yang, E. J., Nishino, S., Chung, K. H., et al. (2015). Regional productivity of phytoplankton in the Western Arctic Ocean during summer in 2010. *Deep Sea Research Part II: Topical Studies in Oceanography*, *120*, 61–71. https://doi.org/10.1016/j.dsr2.2014.11.023

Zhang, X., Walsh, J. E., Zhang, J., Bhatt, U. S., & Ikeda, M. (2004). Climatology and interannual variability of Arctic cyclone activity: 1948–2002. *Journal of Climate*, *17*, 2300–2317. https://doi.org/10.1175/1520-0442(2004)017<2300:CAIVOA>2.0.CO;2

Zhuang, Y., Jin, H., Chen, J., Li, H., Ji, Z., Bai, Y., & Zhang, T. (2018). Nutrient and phytoplankton dynamics driven by the Beaufort Gyre in the western Arctic Ocean during the period 2008–2014. *Deep Sea Research Part I: Oceanographic Research Papers*, *137*, 30–37. https://doi.org/10.1016/j.dsr.2018.05.002